JOURNAL OF GEOPHYSICAL RESEARCH, VOL. 107, NO. B8, 10.1029/2001JB001051, 2002

Post-1906 stress recovery of the San Andreas fault system calculated from three-dimensional finite element analysis

Tom Parsons

U.S. Geological Survey, Menlo Park, California, USA

Received 23 August 2001; revised 26 January 2002; accepted 31 January 2002; published 22 August 2002.

[1] The M = 7.8 1906 San Francisco earthquake cast a stress shadow across the San Andreas fault system, inhibiting other large earthquakes for at least 75 years. The duration of the stress shadow is a key question in San Francisco Bay area seismic hazard assessment. This study presents a three-dimensional (3-D) finite element simulation of post-1906 stress recovery. The model reproduces observed geologic slip rates on major strike-slip faults and produces surface velocity vectors comparable to geodetic measurements. Fault stressing rates calculated with the finite element model are evaluated against numbers calculated using deep dislocation slip. In the finite element model, tectonic stressing is distributed throughout the crust and upper mantle, whereas tectonic stressing calculated with dislocations is focused mostly on faults. In addition, the finite element model incorporates postseismic effects such as deep afterslip and viscoelastic relaxation in the upper mantle. More distributed stressing and postseismic effects in the finite element model lead to lower calculated tectonic stressing rates and longer stress shadow durations (17–74 years compared with 7–54 years). All models considered indicate that the 1906 stress shadow was completely erased by tectonic loading no later than 1980. However, the stress shadow still affects present-day earthquake probability. Use of stressing rate parameters calculated with the finite element model yields a 7–12% reduction in 30-year probability caused by the 1906 stress shadow as compared with calculations not incorporating interactions. The aggregate interaction-based probability on selected segments (not including the ruptured San Andreas fault) is 53–70% versus the noninteraction range of 65–77%. *INDEX TERMS:* 8164 Tectonophysics: Stresses—crust and lithosphere; 7218 Seismology: Lithosphere and upper mantle; 8150 Tectonophysics: Plate boundary—general (3040); 7260 Seismology: Theory and modeling; 7223 Seismology: Seismic hazard assessment and prediction; *KEYWORDS:* stressing rate, San Andreas fault, 1906 earthquake, earthquake interaction, earthquake probability

1. Introduction

[2] On 18 April 1906, a M = 7.8 earthquake and subsequent fire destroyed much of the city of San Francisco, killing as many as 2000–3000 people [e.g., *Ellsworth*, 1990]. The effect on the city from the 1906 earthquake is clearly seen to this day in its architecture. Also clear is its effect on regional seismicity. A rate comparison of $M \geq 6$ earthquakes in 75-year periods before and after 1906 reveals a 14-fold decrease following the great shock (Figure 1) [*Bakun*, 1999]. Termed a stress shadow by *Harris and Simpson* [1998], the inhibition of earthquakes is explained by regional release of accumulated stress during the 1906 earthquake. Urbanization of the San Francisco Bay region, swelling of its population, and development into a technological center coincided with seismic quietude; this evolution may not have occurred if there were 14 $M \geq 6$ earthquakes in the 20th century as in the 19th century. In this paper I use finite element analysis to address the question, how long might the San Francisco Bay area earthquake respite last?

1.1. Earthquake Interactions, Stress Changes, and Clock Changes

[3] In this section, background information is provided on how earthquake interactions and stress changes are incorporated into probability calculations and on the importance of the tectonic stressing rate in these calculations. An earthquake can be modeled as a slipping dislocation in an elastic half-space [e.g., *Okada*, 1992], enabling estimation of stress transfer to other faults. Calculated changes in stress tensor components are resolved on planes of interest, and changes in failure stress are related to triggering or inhibition of future earthquakes. Usually, the Coulomb stress change is calculated and used to explain patterns of seismicity [e.g., *Yamashina*, 1978; *Das and Scholtz*, 1981; *Stein and Lisowski*, 1983; *Stein*, 1999]. The Coulomb failure criterion (ΔCF) is defined by $\Delta \mathrm{CF} \equiv |\Delta\bar{\tau}_f| + \mu(\Delta\sigma_n + \Delta p)$, where $\Delta\bar{\tau}_f$ is the change in shear stress on the receiver fault (set positive in the direction of fault slip), μ is the coefficient of friction, $\Delta\sigma_n$ is the change in normal stress acting on the receiver fault (set positive for unclamping), and Δp is pore pressure change.

[4] When a Coulomb stress change calculation is made for right-lateral strike-slip faults adjacent to the 1906 earthquake rupture, a stress reduction, or stress shadow is noted

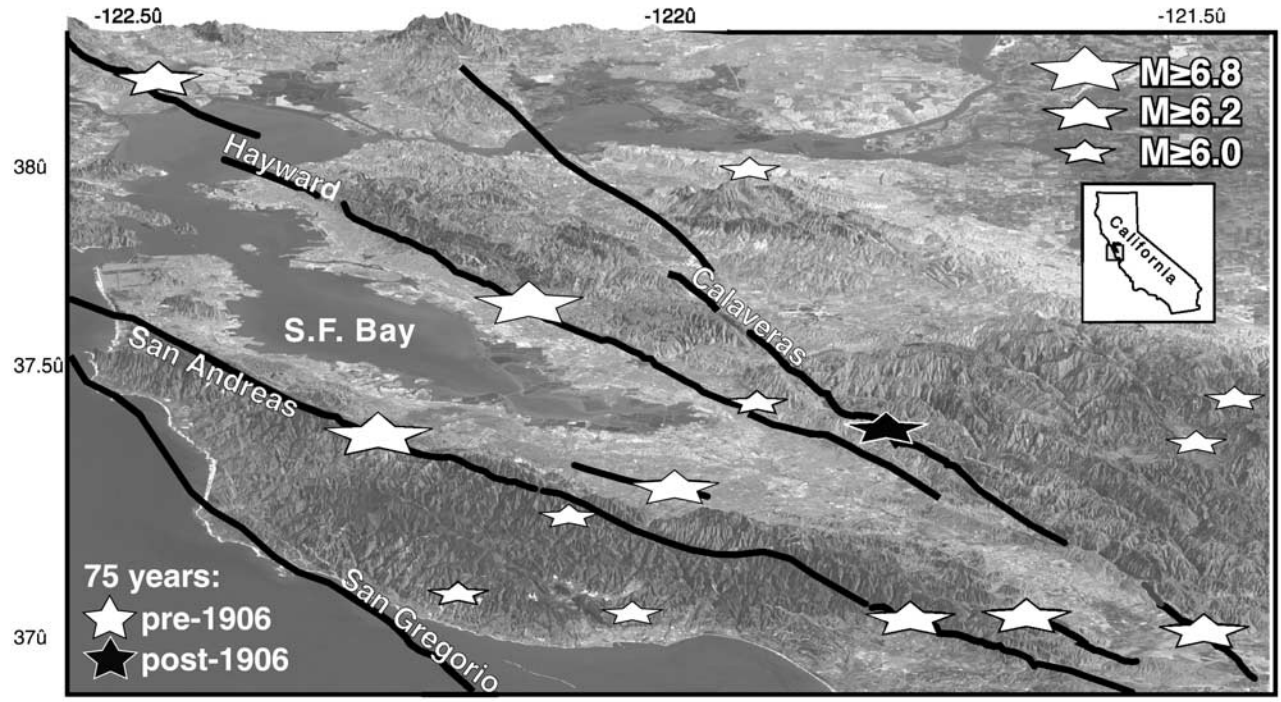

Figure 1. Major faults of the San Francisco Bay area shown with earthquake epicenters $M \geq 6$ [*Bakun*, 1999; *Stein*, 1999] from 75-year periods before (open stars) and after (solid star) 1906. A 14-fold rate decrease of large earthquakes is attributable to stress reduction by the 1906 earthquake [*Harris and Simpson*, 1998].

throughout the San Francisco Bay area [*Harris and Simpson*, 1998]. The calculated stress shadow correlates well with the pronounced reduction in seismicity rate after 1906 (Figure 1). Coulomb stress reduction on a fault may delay an impending earthquake by the time necessary for stress regeneration. The delay, or clock change, (T') can be estimated by dividing the stress change (ΔCF) by the tectonic stressing rate ($\dot{\tau}$), as $T' = \Delta\mathrm{CF}/\dot{\tau}$. Thus the duration of a stress shadow can be known if the tectonic loading rate is known. A simple way to incorporate earthquake interaction into time-dependent probability calculations is to accrue probability from the last earthquake time adjusted by the clock change ($T_0 + T'$) [e.g., *Working Group on California Earthquake Probabilities*, 1990] (Figure 2).

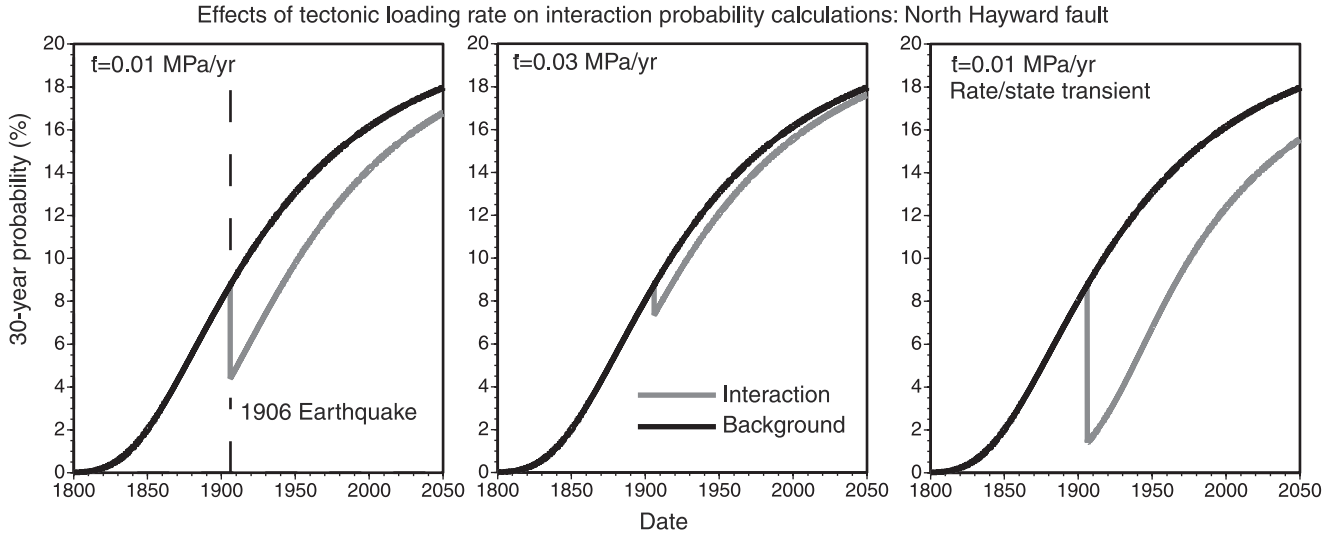

Figure 2. Sample time-dependent earthquake probability calculations made assuming different tectonic loading rates, and hence different durations of the 1906 stress shadow, on the north Hayward fault. The curves show 30-year probability versus time, assuming the last earthquake occurred in 1775. A calculation is also made using a transient, Omori law seismicity rate change as implemented by *Dieterich and Kilgore* [1996], which depends on fault stressing rate.

Alternatively, the earthquake recurrence interval γ can be adjusted by the clock change as $\gamma = \gamma_0 + T'$.

[5] The rate that faults are stressed by tectonic loading is an essential parameter for assessing hazard when earthquake interactions have occurred. Confidence in stress change calculations has grown through repeated correlation with seismicity rate changes [e.g., *Harris*, 1998, and references therein]. Less is understood about tectonic stressing of individual faults. This study builds on previous finite element modeling of California and the San Francisco Bay region [*Ben-Zion et al.*, 1993; *Furlong and Verdonck*, 1994; *Bird and Kong*, 1994; *Reches et al.*, 1994; *Wang et al.*, 1995; *Wang and Cai*, 1997; *Kenner and Segall*, 1999; *Geist and Andrews*, 2000] and is conducted for the purpose of determining tectonic stressing rates for seismic hazard application.

1.2. Model Dependence of Calculated Stress Distribution

[6] The San Francisco Bay area rests atop a broad plate boundary, and it remains unclear how plate boundary stress is transferred to seismogenic faults [e.g., *Lisowski et al.*, 1991; *Savage et al.*, 1999]. Geodetic measurements in the San Francisco Bay region show that the interseismic strain field is diffuse and not concentrated at faults [e.g., *Williams*, 1995; *Savage et al.*, 1999; *Prescott et al.*, 2001]. Stressing rates on vertical faults can be calculated with deep, creeping dislocations located beneath locked faults [e.g., *Simpson and Reasenberg*, 1994; *Stein et al.*, 1997]. Such modeling may be achieved using elastic methods [e.g., *Okada*, 1992]. However, the San Francisco Bay region presents difficulties because there are numerous sources of feedback and interaction that may impact tectonic stressing. As shown in Figure 1, there are four major, nearly parallel right-lateral strands of the San Andreas fault system that cross through the Bay area: from west to east they are the San Gregorio, San Andreas, Hayward, and Calaveras faults. The 1906 stress shadow is ample evidence that an earthquake on one fault affects others; the 1989 $M = 7.1$ Loma Prieta earthquake also changed seismicity rates on neighboring faults [*Reasenberg and Simpson*, 1992; *Parsons et al.*, 1999].

[7] Different techniques for stressing rate calculations result in very different distributions of lithospheric stress. A model of tectonic loading by deep, aseismic fault slip causes the crust intervening between faults to carry less plate boundary stress than at the faults (Figure 3). That stress distribution may be difficult to reconcile with conclusions that the San Andreas and related faults are weak with low friction coefficients [e.g., *Lachenbruch and Sass;* 1980; *Zoback*, 1991; *Reasenberg and Simpson*, 1992; *Bird and Kong*, 1994; *Miller*, 1996; *Geist and Andrews*, 2000], and would be expected to support relatively less stress than the surrounding crust. Tectonic stressing modeling that incorporates whole lithosphere deformation shows a more uniform crustal stress distribution (Figure 3).

[8] In addition to issues of elastic interaction and stress distribution during tectonic loading, there may be important contributions to fault stressing from anelastic processes. Postearthquake afterslip and viscoelastic relaxation of the lower crust and upper mantle are thought to redistribute stress into the seismogenic crust over time [e.g., *Nur and Mavko*, 1974; *Savage and Prescott*, 1978]. Viscoelastic deformation may also play an important role in distributing tectonic stress into the seismogenic crust. Thus a three-dimensional finite element model of the San Francisco Bay area was constructed to incorporate fault interactions, afterslip, and viscoelastic relaxation in modeling pre- and post-1906 fault stressing rates for the San Francisco Bay area. Use of finite elements means that coseismic elastic stress changes can be seamlessly melded with postseismic viscoelastic stress changes. A three-dimensional model allows the influence of fault bends and junctions on stressing rates to be accounted for. Tectonic loading is accomplished by remotely moving one plate past another, which unlike dislocation models, means no assumptions are made as to whether local loading is driven from below or within the lithosphere.

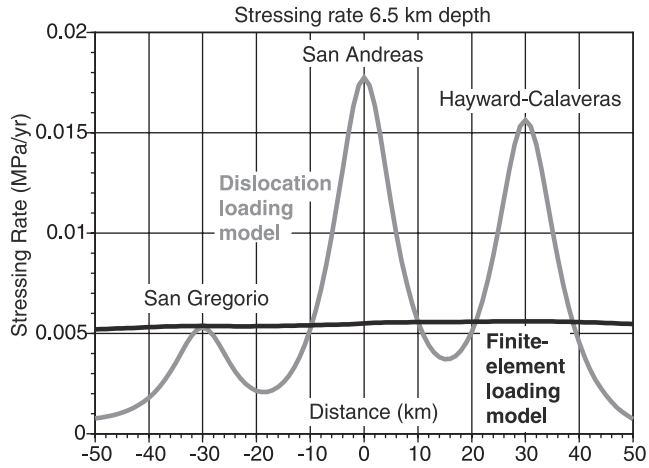

Figure 3. Modeled shear stress distribution in the crust resulting from deep dislocation slip loading and from a 3-D finite element model of plate interactions. Both models fit observed fault slip rates [e.g., *Working Group on California Earthquake Probabilities*, 1999], but the methods predict very different stress distributions as the example profile plotted for 6.5 km depth demonstrates. The dislocation model has 100-km-deep elastic dislocations arranged beneath each parallel right-lateral fault, which slip at observed long-term rates. Shear stressing rates are greatest on the locked faults above the dislocations and drop substantially in the crust between the faults. Nearly all the plate boundary stress is carried on the presumed weak [e.g., *Lachenbruch and Sass*, 1980; *Zoback*, 1991; *Reasenberg and Simpson*, 1992; *Miller*, 1996; *Geist and Andrews*, 2000] transform faults. A contrasting approach, based on finite element modeling discussed in this paper, stresses the whole crust more uniformly; consequently, the faults are stressed at lower rates.

2. A Finite Element Model of the San Francisco Bay Area Lithosphere

[9] A finite element model was constructed to determine the rate of tectonic stressing on San Francisco Bay area faults and to model the stress recovery following the 1906 earthquake. The model incorporates five key features: (1) the Pacific plate moves past the North American plate at ~39 mm/yr on a N34°W oriented vector [e.g., *De Mets et al.*, 1994; *Savage et al.*, 1999], (2) the San Francisco Bay region is crossed by near-vertical strike-slip faults that cut

Table 1. Material Constants Used in the Three Layers of the Finite Element Model[a]

	Layer 1		Layer 2		Layer 3	
Parameter	0–12.5 km	Source	12.5–25 km	Source	>25 km	Source
E, Young's modulus, MPa	8×10^4	1	9×10^4	1	1.9×10^5	1
A, elastic constant, MPa^{-n} s^{-1}	2.0×10^{-4}	2	6.3×10^{-2}	5	5.0×10^3	6
n, elastic constant	1.9	2	3.1	5	3.8	6
Q_c, activation energy, kJ/mol	140.6	2	276	5	492	6
ν, Poisson's ratio	0.25	3	0.26	3	0.28	3
ρ, density, $\times 10^3$ kg/m^3	2.7	4	2.8	4	3.0	4

[a] Elements in the model are all viscoelastic, with viscous behavior controlled by the temperature gradient and the listed constants. References: 1, *Birch* [1966]; 2, *Hansen and Carter* [1983]; 3, *Christensen* [1996]; 4, *Christensen and Mooney* [1995]; 5, *Caristan* [1982]; 6, *Carter and Tsenn* [1987].

through the crust [*Holbrook et al.*, 1996; *Henstock et al.*, 1997; *Parsons and Hart*, 1999] and slip at measured long-term rates [e.g., *Working Group on California Earthquake Probabilities*, 1999] with low friction [e.g., *Lachenbruch and Sass;* 1980; *Zoback*, 1991; *Reasenberg and Simpson*, 1992; *Bird and Kong*, 1994; *Miller*, 1996; *Parsons et al.*, 1999; *Geist and Andrews*, 2000], (3) the crustal velocity structure is known [*Holbrook et al.*, 1996; *Hole et al.*, 2000], and elastic parameters can be inferred, (4) the crustal geotherm is derived from surface heat flow (C. Williams, personal communication, 1999), and from laboratory studies of rock samples the expected viscoelastic response of the lithosphere is derived, and (5) geodetic observations constrain the breadth and rate of combined interseismic elastic and ductile strain [*Lisowski et al.*, 1991; *Williams*, 1995; *Savage et al.*, 1999; *Prescott et al.*, 2001].

2.1. Model Construction

[10] The finite element model of the San Francisco Bay region was built in three compositional layers inferred from

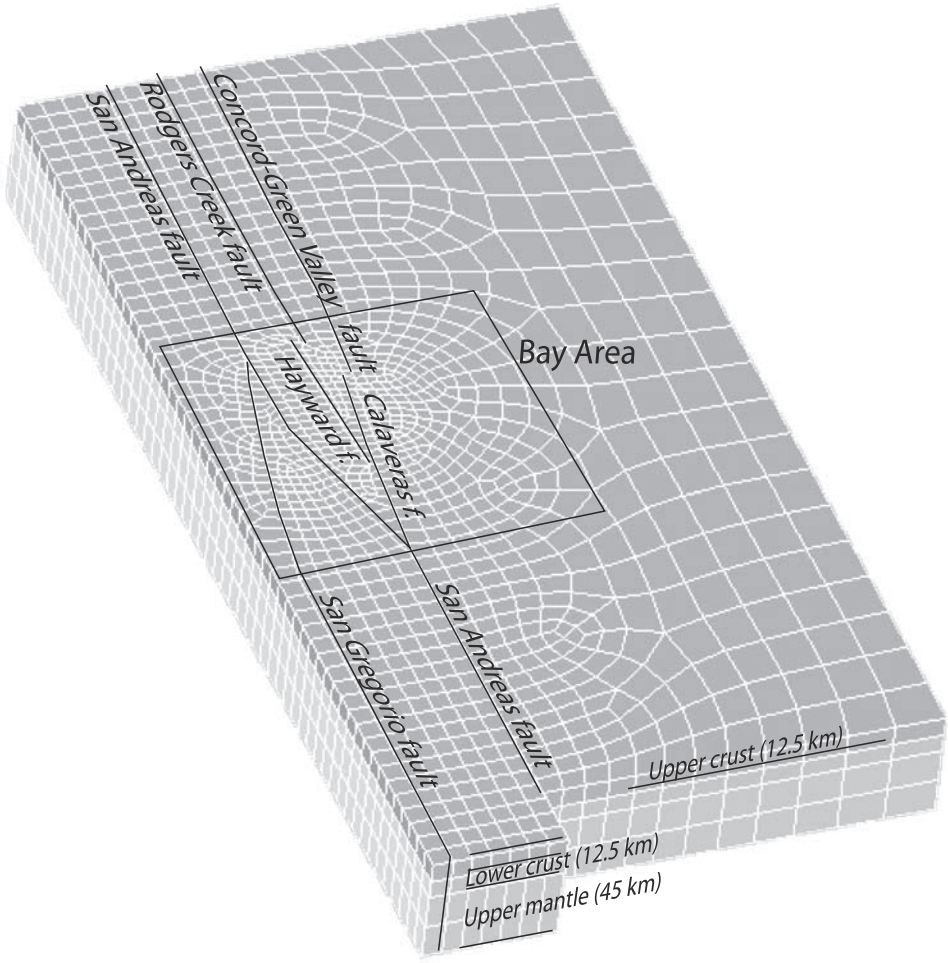

Figure 4. The finite element mesh, model boundaries, and fault structures. The San Francisco Bay area is outlined by a box. Elements are all viscoelastic and have eight nodes located at the corners. The faults are discontinuities in the model and have deformable contact elements on their surfaces that obey a Coulomb failure criterion.

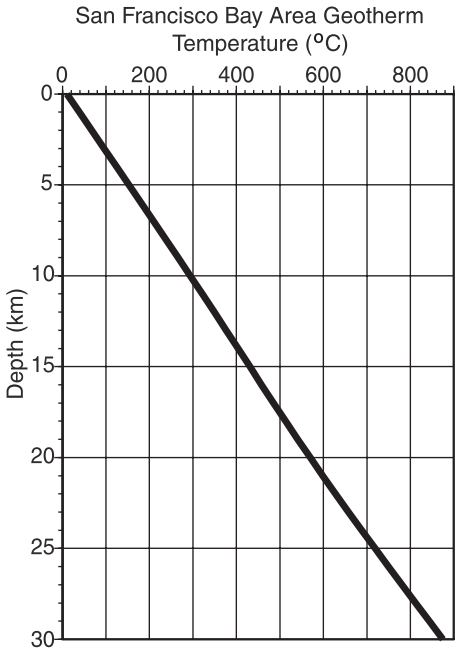

Figure 5. The geothermal gradient used in the model input to the creep equation that controls material behavior (C. Williams, personal communication, 1999). Model elements behave according to Hook's law where temperatures are low and become transitionally more viscoelastic at higher temperatures.

measured crustal velocity structure [e.g., *Holbrook et al.*, 1996; *Hole et al.*, 2000]. Rock composition determines material elastic constants and, consequently, the strain response to an imposed stress at a given rate and temperature. The finite element model is stratified, but as will be described, these layers are not necessarily abrupt boundaries from elastic to viscoelastic behavior. The upper 12.5 km of the model represent Franciscan rocks of accreted origin. This assemblage contains fragments of oceanic crust, pelagic sedimentary rocks, and land-derived marine sandstones and shales mixed together in a melange [e.g., *Page*, 1992]. Elastic properties of these rocks were approximated by wet Westerly granite and are given in Table 1. The lower crust is also 12.5 km thick in the model and has elastic properties representative of basalt-diabase composition [*Brocher et al.*, 1994]. The upper mantle layer has properties associated with an average of wet and dry dunite samples (Table 1) and is 45 km thick, which is required to maintain isostatic balance with the crustal column at or near sea level [*Lachenbruch and Morgan*, 1990].

[11] The model is composed entirely of eight-node viscoelastic elements (Figure 4). It consists of 8052 elements with 7200 active nodes having a combined 18810 degrees of freedom (*ux*, *uy*, and *uz*). The proportion of viscous to elastic behavior of a given element node is governed by the local crustal geotherm derived from heat flow measurements (C. Williams, personal communication, 1999) (Figure 5). Temperature dependence of strain rate $\dot{\varepsilon}$ in the model is controlled by the creep equation [e.g., *Kirby and Kronenberg*, 1987]

$$\dot{\varepsilon} = A \exp(-Q_c/RT)\sigma^n, \tag{1}$$

where A, Q_c (activation energy), and n are experimentally derived elastic constants, R is the universal gas constant, T is temperature, and σ is differential stress (Table 1). Equation (1) causes a transition from elastic to ductile strain with increasing temperature (Figures 5 and 6). There is a less abrupt change from elastic to ductile deformation than if layer viscosities were assigned or if elastic elements were layered above viscoelastic elements. An attempt is made to replicate the observed crustal transition from seismogenic strain in the shallow crust to aseismic creep in the lower crust and upper mantle [e.g., *Hill et al.*, 1990]. The varying elastic constants associated with the upper crustal, lower crustal, and upper mantle model layers do cause small rheological discontinuities at the layer boundaries, particularly between the upper and lower crust (Figure 6).

[12] The finite element model has cuts in it that represent the major strike-slip faults of the San Francisco Bay region (Figures 1 and 4). The faults are deformable and are constructed from contact elements that obey the Coulomb failure relation

$$\mathrm{CF} \equiv \bar{\tau}_f + \mu(\sigma^n), \tag{2}$$

where $\bar{\tau}_f$ is the shear stress acting on a fault surface, μ is the friction coefficient, and σ_n is the component of stress acting normal to a fault surface. Contact elements have zero thickness and are welded to the sides of viscoelastic elements. The faults are all throughgoing [e.g., *Holbrook et al.*, 1996; *Henstock et al.*, 1997; *Parsons and Hart*, 1999]

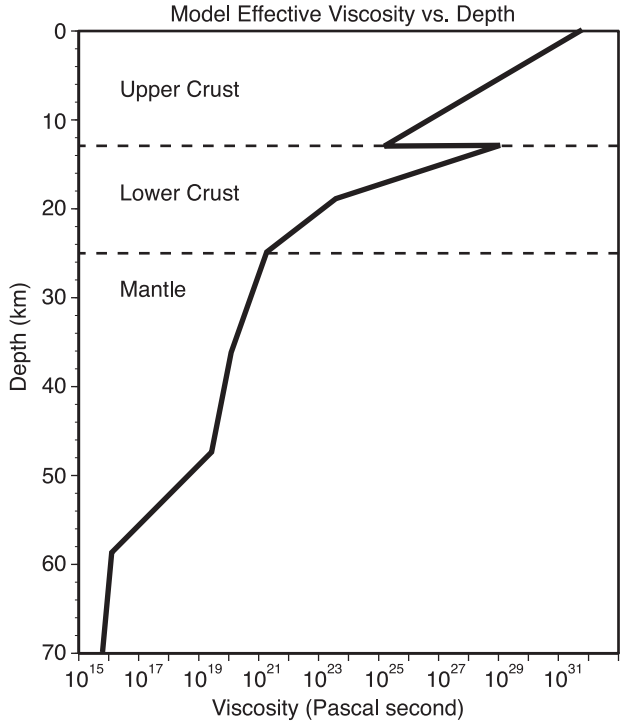

Figure 6. Effective viscosity versus depth. Viscosity is calculated from $n = \sigma^{1-n} \exp(Q_c/RT)/2A$, where σ is differential stress (calculated with the finite element model), R is the gas constant, and Q_c (activation energy), A, and n are experimentally determined values (Table 1). Most of the strength in the model is carried in the crust because a partially wet upper mantle rheology is used.

and penetrate into the mantle. Faults are permitted to slip down to the 70-km base of the model, but as will be shown, they do not slip anywhere in the mantle because the very high confining pressure clamps them. The initial fault friction coefficients were set to a low value of 0.1 [e.g., *Lachenbruch and Sass;* 1980; *Zoback*, 1991; *Reasenberg and Simpson*, 1992; *Miller*, 1996; *Parsons et al.*, 1999; *Geist and Andrews*, 2000]. Fault friction coefficients were modified slightly to match observed long-term slip rates as described in section 3.1.

2.2. Boundary Conditions, Loads, and Calculations

[13] The model edges are oriented parallel and orthogonal to the Pacific–North American relative plate motion vector of ~N34°W [e.g., *De Mets et al.*, 1994] (Figure 4). Following *Geist and Andrews* [2000], tectonic stressing is emulated by moving the western edge and the southern edge of the model west of the San Andreas fault at a 39 mm/yr rate. The eastern model edge is held fixed to North America and is thus not free to move laterally. The model base is freely slipping laterally but cannot move vertically. Models up to 200 km thick were tested to determine if the bottom boundary condition affects results; the high regional geotherm (Figure 5) causes very low mantle viscosity below ~60 km, and thus additional thickness beyond 60–70 km has no effect (Figure 6). The northern and southern model faces are deformable only parallel to their surfaces. The model free surface is fully deformable. All velocity constraints are imposed on the model edges as described above; no constraints are imposed on elements within the model. Before any Pacific–North American plate motion is introduced, the model is subjected to gravity for a 10,000-year period required to fully compress under its own weight.

[14] All modeling presented here was conducted using the ANSYS® finite element program. ANSYS® employs the Newton-Raphson approach to solve nonlinear problems. In this method a load is subdivided into a series of increments applied over several steps. Before each solution the Newton-Raphson method evaluates the out-of-balance load vector, which is the difference between the restoring forces (the loads corresponding to the element stresses) and the applied loads. A linear solution is performed, using the out-of-balance loads, and checks for convergence. If convergence criteria are not satisfied, the out-of-balance load vector is reevaluated, the stiffness matrix updated, and a new solution is obtained. The system of equations is solved through direct elimination of equations until the problem converges (sparse direct solver).

[15] The finite element model presented here shares features associated with the viscoelastic coupling model of *Savage and Prescott* [1978] and *Thatcher* [1983] wherein surface deformation does not depend on whether motion is driven by the ductile mantle (elastic plates are dragged passively by an active upper mantle) or loading through the elastic plates over a passive mantle. In the finite element model, the distribution of stressing at the plate boundary faults is not presupposed. However, a choice is made to apply remote plate boundary stressing using velocity boundary conditions, effectively creating a viscoelastic shear zone model as suggested by *Pollitz* [2001]. The stress distribution is determined by the relative yield strengths of the different materials. Thus the model transfers stress most rapidly through the relatively strong crust (Figure 6).

[16] The finite element model was constructed in a forward sense using known or inferred lithospheric characteristics of the San Francisco Bay region. With the exception of slight modifications to fault friction coefficients (described below), the fundamental aspects of the model as presented here are unchanged throughout all calculations.

3. Tests of the Finite Element Model

[17] Two tests were conducted before the San Francisco Bay region finite element model was used to model tectonic stressing rates. The model was required to satisfy geologically determined, long-term fault slip rates, and shorter-term geodetic observations of regional deformation. Below, these two exercises are described.

3.1. Long-Term Fault Slip Observations

[18] The finite element model was constrained to match observed long-term fault slip rates within given error ranges. Long-term fault slip rates derived from geological observations in the San Francisco Bay area were compiled by the *Working Group on California Earthquake Probabilities* [1999] (Figure 7). An initial friction coefficient of $\mu = 0.1$ was used on all faults, and the Pacific plate was moved 39 mm/yr for a 1000-year period at 10-year time steps. Slip rates stabilized within a few hundred years with slightly too much slip on the San Andreas and San Gregorio faults and not enough on the Hayward and Calaveras faults. A stable model was developed that matched observed slip rates (Figure 7) by iterating forward models with adjusted friction coefficients. Friction coefficients of $\mu = 0.1$ were retained for the Hayward, Calaveras, and creeping section of the San Andreas (south of its junction with the Calaveras) faults. Slip within the San Andreas fault system was best fit using a coefficient of $\mu = 0.132$ for the San Francisco Peninsula segment of the San Andreas fault, and $\mu = 0.125$ for the San Gregorio fault. These friction coefficients are slightly higher than, but comparable to, those modeled by *Geist and Andrews* [2000].

[19] In the finite element model a balance of slip between the faults is attained because each fault zone has features that encourage and inhibit slip relative to the others. The San Gregorio and peninsular San Andreas faults are not ideally aligned with the relative plate motion vector and were given slightly higher friction coefficients. The San Gregorio fault might absorb more slip except that it terminates at the south model edge [*Geist and Andrews* 2000] and joins the San Andreas to the north. These traits shift some slip east to the better aligned, lower friction Hayward and Calaveras faults (Figure 7). However, the Hayward and Calaveras faults have significant ($\geq$5 km offset) interruptions and step over zones that act to retard slip, preventing these faults from absorbing all the relative plate motion. Thus a slip balance is set up in the model that matches observed values.

[20] In the long-term fault slip simulation, the faults were permitted to slip at all depths (0–70 km). However, in the model, fault slip only occurred at middle to upper crustal depths (0–12.5 km). Increasing temperature and compositional changes in the lower crust and upper mantle parts of the model caused strain accommodation to occur by viscoe-

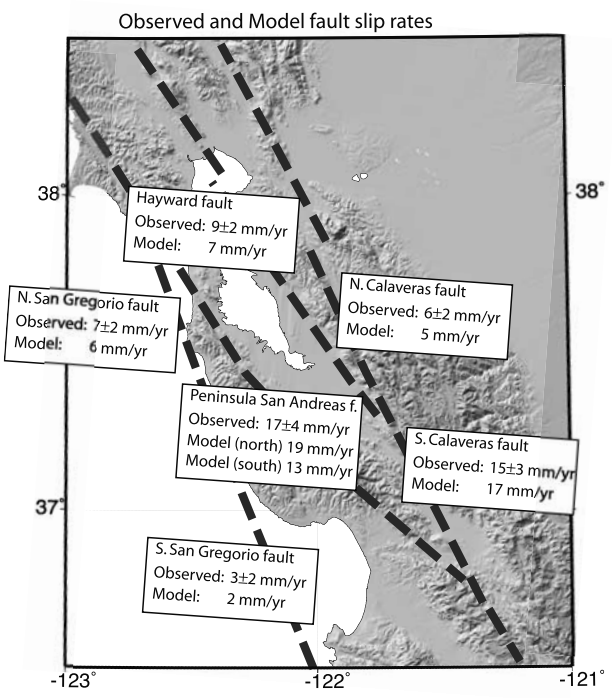

Figure 7. Comparison between observed long-term fault slip rates [*Working Group on California Earthquake Probabilities*, 1999] and slip rates calculated with the finite element model. Fault friction was varied iteratively to match observed slip rates and varies from $\mu = 0.1$ on the Hayward and Calaveras faults to $\mu = 0.132$ on the peninsular San Andreas fault.

lastic deformation of elements. The deeper, less viscous elements have lower yield strength than even the low-friction faults. As will be shown, deep, postseismic afterslip was observed in the model (limited to the lower crust) following a simulation of the 1906 earthquake.

3.2. Interseismic Geodetic Observations

[21] Matching long-term fault slip with the finite element model provides a test of fault geometry, friction, and seismic strain. Shorter-term geodetic observations measure the interseismic strain field, a combination of the Earth's shallow elastic deformation with the deeper, ductile response to relative plate motions that occurs while the faults in the seismogenic crust are largely locked. If geodetic observations can be fit, then a degree of confidence in the viscoelastic finite element model is conferred.

[22] To test the model against geodetic observations, faults were locked from the surface to 12.5 km, except for the creeping segment of the San Andreas fault south of its junction with the Calaveras fault, which was left unlocked. The model was run for a few hundred years to stabilize the shear stressing rates, and then the Pacific plate continued to be moved 39 mm/yr relative to North America at 0.5-year time steps for 50 years (providing a span that encompasses all modern geodetic observation intervals). Global Positioning System (GPS) velocity data from two campaigns across the southern and central San Francisco Bay area (U.S. Geological Survey automatic processing) were compared with nearest nodes in the finite element model (Figure 8). Observed and modeled vectors are in reasonable accordance, particularly west of the Hayward and Calaveras faults (Figure 8a). Mismatches are greatest east of the Calaveras fault because of two features not incorporated in the finite element model: Hayward and Calaveras fault creep [e.g., *Simpson*, 2000], and compositional and thermal differences between the Bay area and Great Valley lithosphere [e.g., *Hill et al.*, 1990; *Hole et al.*, 2000]. A velocity profile calculated orthogonal to the relative plate motion vector from trilateration data [*Lisowski et al.*, 1991] is also fit by the finite element model (Figure 8b).

[23] The finite element model has one-dimensional structure and thermal characteristics, yet can reproduce most of the observed interseismic deformation, and with minor variations made to fault friction coefficients, long-term geologic fault slip rates. A model that replicates observed crustal strain rates should be useful in modeling crustal stressing rates. In section 4, fault stressing rates before and after the 1906 earthquake are determined using the finite element model.

4. Stressing Rate Results

[24] Tectonic stressing is simulated with the finite element model of the San Francisco Bay region by moving the Pacific plate past the North American plate. Interseismic stressing is modeled by locking all faults (except the creeping section of the San Andreas) to a 12.5 km depth. The deeper parts of the faults are permitted to slip, and the lower crust and upper mantle deform viscoelastically. Tectonic motions are applied for a 300-year period in the model. After 300 years the 1906 earthquake is simulated by displacing the San Andreas fault with the slip distribution of *Thatcher et al.* [1997]. Calculations were made for the postseismic 300-year period with and without tectonic motion. Stressing rates before and after the 1906 earthquake can be compared, and postseismic effects can be examined with and without the contribution of tectonic stressing. A full stress history is retained for each model node and on each contact surface. In section 4.1 a patch of the northern Hayward fault is examined in detail to provide an example of the model results and to describe different modeled stressing behaviors resulting from tectonic motions and the 1906 earthquake.

4.1. Example: Pre- and Post-1906 Stressing of the North Hayward Fault

[25] The Hayward fault in combination with the Rodgers Creek fault (Figures 1 and 4) was assigned the highest 30-year probability (32%) of rupturing a $M \geq 6.7$ earthquake in the San Francisco Bay area by the *Working Group on California Earthquake Probabilities* [1999]. The north Hayward fault is also calculated to be one of the most strongly affected by the 1906 earthquake. I thus focus on this fault as a relevant and expository case study. After discussing the pre-1906 stressing rate I describe three key features of the post-1906 response that affect stress recovery on the Hayward fault: (1) coseismic static stress change, (2) deep afterslip on the San Andreas fault with associated lower crustal relaxation, and (3) upper mantle stress diffusion and redistribution.

[26] The pre-1906 stressing rate on the north Hayward fault from finite element modeling is 0.010 MPa/yr (Figure 9 and Table 2). The stressing rate is constant and independent

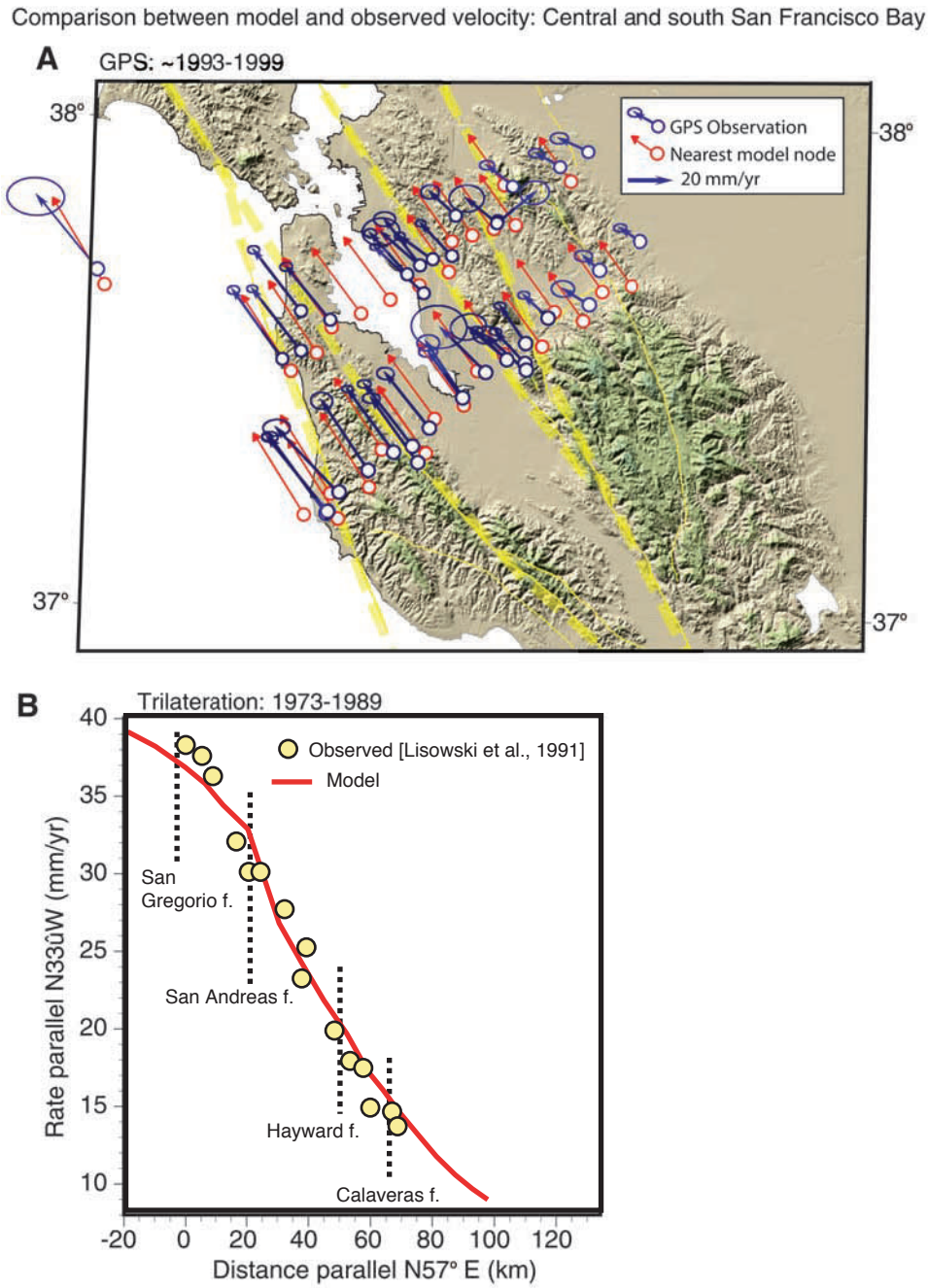

Figure 8. (a) Comparison between GPS velocity vectors (U.S. Geological Survey automatic processing) in the central and southern San Francisco Bay area with velocities at nearest model nodes. Magnitudes and directions are reasonably well matched west of the Calaveras fault. The fit is poorer in the Great Valley, perhaps because of changes in lithospheric character not reflected in the finite element model. (b) Relative PacificñNorth American plate rate from trilateration plotted orthogonal to the relative motion vector [Lisowski et al., 1991] is well fit by the finite element model.

of the absolute stress state. Deviation from this rate occurs only when the model is run for thousands of years with locked faults, causing elements intervening between the major faults to reach their elastic limit, after which they refer stress onto the strike-slip faults. In the real Earth these stresses would be relieved by slip on minor accommodating faults in places such as fault step over zones or restraining and releasing bends.

[27] Following a 300-year stress buildup, the 1906 earthquake was simulated by rapidly slipping the San Andreas fault using the slip distribution of Thatcher et al. [1997]. After the 1906 earthquake simulation a static Coulomb stress drop occurred on most San Francisco Bay area fault planes comparable to calculations by Harris and Simpson [1998]. The stress shadow is especially apparent on the north Hayward fault where Coulomb stress

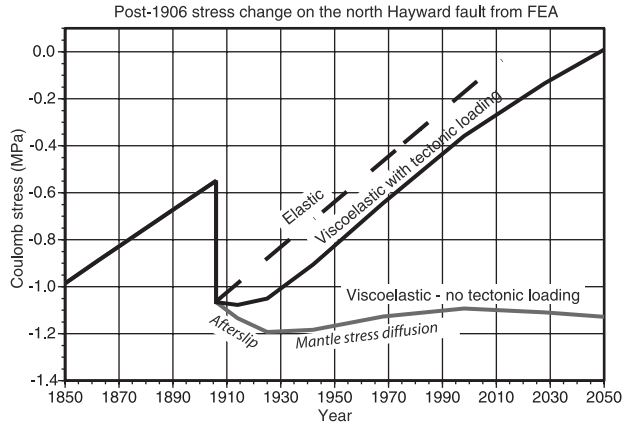

Figure 9. Coulomb stress plotted as a function of time for a point on the north Hayward fault (0–6.25 km depth) estimated with the finite element model. Stress increases because of relative plate motion until the 1906 earthquake is simulated, after which a ~0.55 MPa static stress drop is incurred. Three different stress histories diverge; the solid black line shows a combination of tectonic stressing, postseismic afterslip, and deep crustal/upper mantle relaxation calculated by simulating the 1906 earthquake with continuous tectonic loading. The gray solid line shows the postseismic effects without tectonic loading, and the dashed black line shows stress recovery only with tectonic stressing, neglecting postseismic effects.

is calculated to be reduced by ~0.55 MPa (Figure 9). Total Coulomb stress is calculated by determining the components of stress parallel to fault sliding direction (shear stress in equation (2)) and oriented normal to the contact elements. Stress change is found by differencing stress between time steps. The 1906 earthquake slip was calculated over a 1-min-long time step in the finite element model. The value found for static Coulomb stress change using total stress in the finite element model ($\Delta CF = -0.546$ MPa) for a patch of the north Hayward fault is the same as calculated with dislocations in an elastic half-space ($\Delta CF = -0.548$ MPa) using the DLC program written by R. Simpson based on the subroutines of *Okada* [1992].

[28] Static stress change from the 1906 earthquake is a coseismic phenomenon well suited to elastic calculations. The viscoelastic characteristics of the finite element model enable longer-term effects of the 1906 earthquake to be considered. After the static stress change a further reduction in Coulomb stress occurs in the model that takes ~20 years to complete (Figure 9). The deeper parts of the San Andreas fault slipped an additional ~1–3 m in the lower crust after the modeled 1906 earthquake (Figure 10). The resulting 0.12-MPa stress drop at the Hayward fault occurs through a combination of elastic and viscoelastic stress transfer from the lower crust. The faults extending into the mantle part of the model do not slip during tectonic loading or after the 1906 earthquake simulation because high ambient stresses act to clamp them shut, and upper mantle tectonic strain occurs by ductile flow.

[29] Termination of fault slip at depth (Figure 10) transfers stress into the upper mantle. With time, heightened stress in the upper mantle is expected to equilibrate and partly diffuse into the crust [e.g., *Nur and Mavko*, 1974; *Savage and Prescott*, 1978]. This effect can be seen in Figure 9, where after the period of stress decrease on the Hayward fault due to San Andreas fault afterslip, the slope of the Hayward fault stressing rate curve is slightly higher than before 1906. The post-1906 duration of this effect at the north Hayward fault is ~60 years, from ~1930 to ~1990 (Figure 9). Stress shadow durations were calculated by continuing tectonic loading after simulation of the 1906 earthquake. Thus the postseismic viscoelastic loading and afterslip effects can be incorporated into the calculated post-1906 fault stressing rates (Figure 9 and Table 2).

[30] The combination of coseismic and postseismic effects calculated for the north Hayward fault can be compared with other analyses. The 3-D finite element model has similar features to the 2-D model of *Kenner and Segall* [1999], who showed initial postseismic shear stress decreases followed by mantle relaxation induced increases of varying magnitude and duration depending on fault configurations. The model presented here has postseismic effects that are closest to a combination of the freely slipping deep faults and crustal shear-zone models tested by *Kenner and Segall* [1999], who did not calculate tectonic loading rates. A 3-D finite element model of the San Francisco Bay region was constructed by

Table 2. Tectonic Loading Rates on Various San Francisco Bay Region Fault Segments[a]

Fault	FEA Stressing Rate, MPa/yr	Dislocation Stressing Rate	1906 Shadow Duration, years		
			Viscoelastic	Elastic	Dislocation
San Andreas Peninsula	0.015	0.025			
San Andreas north	0.025	0.032			
Rodgers Creek	0.017	0.012	34	22	31
Hayward north	0.010	0.015	74	56	37
Hayward south	0.008	0.015	43	31	17
San Gregorio north	0.016	0.014	70	47	54
San Gregorio south	0.014	0.009	19	11	17
Green Valley	0.011	0.007	17	11	17
Concord	0.008	0.007	23	13	15
Calaveras north	0.008	0.011	33	22	16
Calaveras central	0.008	0.018	32	20	9
Calaveras south	0.009	0.024	39	19	7

[a] Rates were calculated with the 3-D finite element model (FEA) and using creeping elastic dislocations located beneath the major fault zones. In general, loading determined with the finite element model is slower because a smaller proportion of the plate boundary stress is focused on faults compared with dislocation loading. The duration of the 1906 stress shadow is given from calculations made by dividing static stress changes by the dislocation and finite element (elastic, no postseismic viscoelastic effects incorproated) loading rates and as modeled incorporating post-1906 afterslip and mantle relaxation effects (viscoelastic).

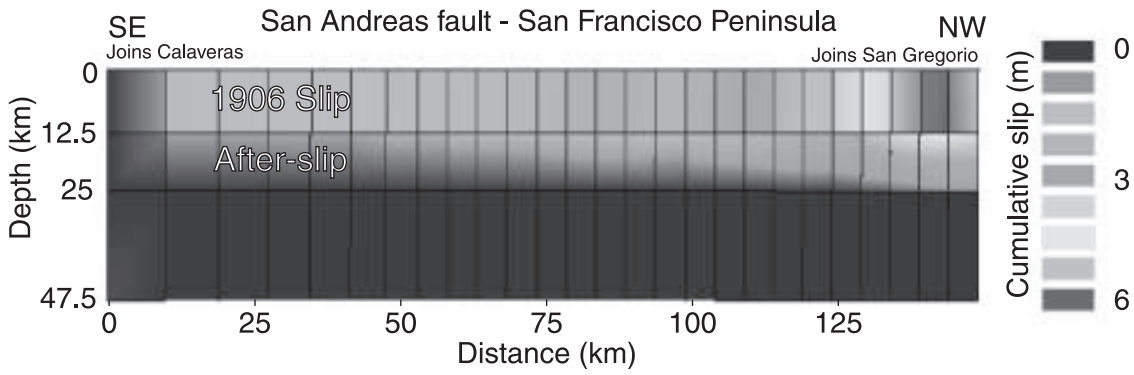

Figure 10. Side view (looking west) at the cumulative slip of the peninsular segment of the San Andreas fault in the finite element model. Coseismic 1906 slip was limited to the upper 12.5 km of the fault. Modeled post-1906 afterslip is evident on the lower crustal extension of the San Andreas fault. No slip occurs on the model faults in the mantle.

Furlong and Verdonck [1994] that compared three different fault configurations: a lower crustal detachment fault connecting the San Andreas and Hayward faults, a completely elastic crust, and a weak lower crust. The tectonic stressing rate calculated by *Furlong and Verdonck* [1994] for the Hayward fault of 0.013 MPa/yr is comparable to the value of 0.010 MPa/yr in this study. The shape of the stressing rate curves calculated by *Furlong and Verdonck* [1994] is similar to those of this study, with their detachment model matching the shadow duration best, probably because the signal of afterslip on vertical planes is difficult to discern from slip on a horizontal plane [e.g., *Lisowski et al.*, 1991].

4.2. Duration of the 1906 Stress Shadow on Major San Francisco Bay Area Faults

[31] The calculated response to the 1906 earthquake on all the major faults in the finite element model (apart from the San Andreas) is similar to that discussed in detail for the north Hayward fault above. The primary difference is the magnitude of the impact (Table 2), which depends on the distance between the target fault and the 1906 rupture. Recovery from the 1906 stress shadow is also calculated with pre-1906 stressing rates, yielding an estimate of its duration if postseismic viscoelastic effects are neglected. These results show the shadow lasting from 11 to 56 years compared with 17 to 74 years if viscoelastic responses are incorporated (Table 2). A dislocation loading model yields a shadow that lasts between 7 and 54 years.

[32] The San Andreas fault north of its junction with the San Gregorio fault (Figure 4) has the fastest calculated stressing rate in the San Francisco bay region at 0.025 MPa/yr, while the Calaveras fault has the slowest at 0.008 MPa/yr. Calculated tectonic stressing rates on faults are half to two thirds of the corresponding values found using dislocations [e.g., *Savage and Lisowski*, 1993; *Simpson and Reasenberg*, 1994; *Working Group on California Earthquake Probabilities*, 1999] (Table 2). A longer calculated duration of the 1906 stress shadow results if lower tectonic stressing rates are used. A longer stress shadow is commensurate with observations that 75 years passed virtually free of large earthquakes in the Bay region (Figure 1).

[33] Differences in the modeled 1906 stress shadow duration resulting from dislocation and finite element techniques are nonuniform. For example, the Rodgers Creek and Green Valley faults are calculated to have nearly the same stress shadow (Table 2), whereas the southern Calaveras and north Hayward faults have substantially different stress recovery times depending on the calculation method. As will be shown, these effects have varying impact on present-day earthquake probability calculations.

4.3. Why Surface Fault Slip Rates Are Not Always Proportional to Tectonic Loading Rates

[34] A paradox arises from comparison of the tectonic stressing rates calculated with the San Francisco Bay region finite element model (Table 2) with the fault slip rates shown in Figure 7. For example, the calculated tectonic stressing rate of the north San Gregorio fault is 0.016 MPa/yr, comparable to the 0.015 MPa/yr rate calculated for the peninsular segment of the San Andreas fault. The fault slip rate for the north San Gregorio fault is calculated to be 6 mm/yr, while the peninsular segment of the San Andreas fault is calculated to slip $\sim$16 mm/yr, more than twice the San Gregorio rate despite comparable friction coefficients.

[35] This paradox can be explained by considering the concept of fault interaction and by examining the San Francisco Bay area fault geometry. The San Andreas is the most continuous fault in the San Francisco Bay region model, and it requires relatively less stress to slip as compared with shorter, subparallel faults that have terminations or sizable step overs ($\geq$5 km offset) like the Hayward and San Gregorio faults. Since the continuous San Andreas fault slips more readily than the other model faults, it can also transfer stress away from those faults, as evidenced by the 1906 stress shadow. A model result is that shorter faults will have slower long-term average surface slip rates even if they are stressed at tectonic rates comparable to longer, fast slipping faults.

5. Impact on Earthquake Probability Calculations

[36] Finite element modeling of the San Francisco Bay region yields slower tectonic stressing rates than are calculated with elastic dislocations because plate boundary stress is distributed more uniformly in the crust instead of just on

Table 3. The 30-year Conditional Earthquake Probability Calculations[a]

Fault	Recurrence, years	Last Earthquake	Stress Change	Probability No Interactions, %	Effects of Different Loading Models on Interation Probability					
					Probability Transient Included, %			Probability No Transient, %		
					FEA Load	Viscoelastic	Dislocation Load	FEA Load	Viscoelastic	Dislocation Load
Rodgers Creek	236	>1730	−0.374	24	21	20	20	21	20	20
Hayward north	295	>1665	−0.560	19	14	13	15	15	14	17
Hayward south	236	1868	−0.248	16	10	9	11	12	11	14
San Gregorio north	438	>1685	−0.752	11	8	7	8	9	8	9
San Gregorio south	615	<1776	−0.154	3–10	2–10	2–10	2–10	2–10	2–10	2–10
Green Valley south	881	<1776	−0.121	0–7	0–7	0–7	0–7	0–7	0–7	0–7
Concord	991	<1776	−0.104	0–6	0–6	0–6	0–6	0–6	0–6	0–6
Calaveras north	324	<1776	−0.176	14–19	12–17	11–17	12–18	12–17	11–17	12–18
Calaveras central	374	<1776	−0.160	11–17	9–16	8–15	9–16	9–16	8–15	9–16
Calaveras south	703	<1776	−0.171	1–9	1–9	1–9	1–9	1–9	1–9	1–9
Aggregate				65–77	56–72	53–70	57–73	59–73	55–72	59–74

[a] Calculations were made for the year 2002 incorporating 1906 stress interactions on selected fault segments identified by the *Working Group on California Earthquake Probabilities* [1999] (WG99) using different tectonic stressing models. "Probability no interactions" means values calculated without any earthquake stress interactions. "FEA load" means application of stressing rates determined with the finite element model with only elastic coseismic stress effects. "Viscoelastic" means 1906 stress shadow durations calculated with elastic coseismic, postseismic afterslip, and stress diffusion effects were used. Probability values calculated with and without a transient, Omori law seismicity rate change effect are included.

the faults (Figure 3). Slower stressing rates mean that the duration of the 1906 stress shadow might be longer than previously thought, reducing the calculated likelihood of present-day San Francisco Bay earthquakes. Here I examine the impact of the 1906 stress shadow on earthquake probability calculations for some of the major San Francisco Bay area fault zones.

[37] In the probability calculations a simplified set of parameters from the *Working Group on California Earthquake Probabilities* [1999] are used with different approaches to stress interaction from the 1906 earthquake. Tectonic loading rates from finite element and dislocation modeling are used to calculate stress recovery times, and post-seismic viscoelastic effects are also incorporated (Table 2). In addition, all values are input with and without a transient, Omori law probability change [see *Dieterich*, 1994; *Dieterich and Kilgore*, 1996] (Table 3).

[38] Following the *Working Group on California Earthquake Probabilities* [1999], I use Brownian Passage Time defined as

$$f(t,\gamma,\alpha) = \left(\frac{\gamma}{2\pi\alpha^2 t^3}\right)\exp\left(\frac{(t-\gamma)^2}{2\pi\alpha^2 t}\right), \qquad (3)$$

where γ is the average interevent time, t is time, and α is the aperiodicity, equivalent to the coefficient of variation in the more familiar lognormal or Weibull probability distributions.

[39] Application of different tectonic and post-1906 stressing models affects San Francisco Bay area fault segment probabilities (Table 3). Probability reduction from the stress shadow varies by ~1–2% per segment for faults with known elapsed time since the last earthquake or for faults with paleoseismological observations (Hayward, Rodgers Creek, San Gregorio) (Figure 11 and Table 3). The differences in probability change due to different loading models is small because of large uncertainty (or no knowledge at all) in the time elapsed since the last large earthquake. In the year 2002, variation resulting from different loading models in the aggregate 30-year probability for all considered fault segments is ~4–6% (Table 3). On all segments, models show complete recovery from the stress shadow through tectonic loading by 1980 at the latest (Table 2). The 1906 stress shadow still causes a ~3–12%

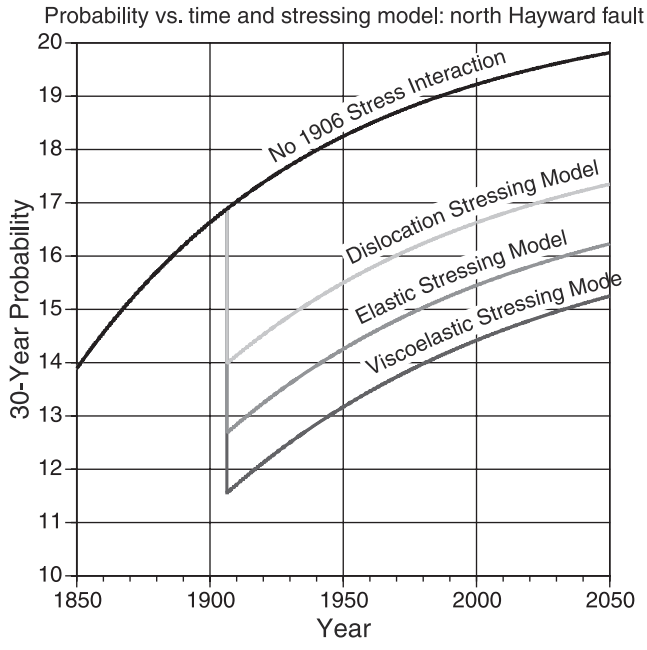

Figure 11. The 30-year probability versus time plotted for the north Hayward fault example. The solid black curve shows probability growth assuming the last earthquake occurred in 1665 (see Table 3 for full details and 2002 values) and without interaction from the 1906 earthquake. The three other curves show the result on probability of applying the stress shadow durations calculated from a dislocation stressing model, and finite element stressing with (viscoelastic) and without (elastic) post-1906 viscoelastic effects such as deep afterslip and lower crustal and upper mantle relaxation.

reduction in the 30-year probability of $M \geq 6.7$ earthquakes on investigated fault segments in the year 2002 (Table 3).

6. Conclusions

[40] A finite element model of pre- and post-1906 tectonic stressing exhibits significantly different characteristics from models using elastic dislocations. Stressing from relative plate motion is distributed throughout the crust, whereas stressing modeled with elastic dislocations is focused on major fault zones (Figure 3). Modeled fault stressing rates are lower if finite elements are used, and the resulting calculated stress shadow from the 1906 earthquake lasts longer on most faults. In addition, postseismic effects simulated with the finite element model such as afterslip and lower crustal relaxation lengthen the duration of the stress shadow more than upper mantle relaxation shortens it. These results may explain the ~75-year period of seismic quiet that followed the 1906 earthquake. Present-day earthquake probability calculations show a persisting effect from the 1906 shadow, with reduced aggregate probability on investigated fault segments ranging from 3% to 12% depending on the stressing model.

[41] **Acknowledgments.** I acknowledge important contributions made to this study by Mark Rodamaker of MCR Associates and interns Nick Kirkman and Rachel Margrett of Brunel University, U.K. Funding from the Pacific Gas and Electric Company and the USGS Coastal and Marine Program is gratefully acknowledged. Improvements to the manuscript were made because of reviews by Eric Geist, Ruth Harris, Liz Hearn, Shelly Kenner, and Ross Stein.

References

Bakun, W. H., Seismic activity of the San Francisco Bay region, *Bull. Seismol. Soc. Am.*, *89*, 764–784, 1999.

Ben-Zion, Y., J. R. Rice, and R. Dmowska, Interaction of the San Andreas fault creeping section with adjacent great rupture zones and earthquake recurrence at Parkfield, *J. Geophys. Res.*, *98*, 2135–2144, 1993.

Birch, F., Compressibility; elastic constants, *Mem. Geol. Soc. Am.*, *97*, 97–173, 1966.

Bird, P., and X. Kong, Computer simulations of California tectonics confirm very low strength of major faults, *Geol. Soc. Am. Bull.*, *106*, 159–174, 1994.

Brocher, T. M., J. McCarthy, P. E. Hart, W. S. Holbrook, K. P. Furlong, T. V. McEvilly, J. A. Hole, and S. L. Klemperer, Seismic evidence for a possible lower-crustal detachment beneath San Francisco Bay, California, *Science*, *265*, 1436–1439, 1994.

Caristan, Y., The transition from high temperature creep to fracture in Maryland diabase, *J. Geophys. Res.*, *87*, 6781–6790, 1982.

Carter, N. L., and M. C. Tsenn, Flow properties of the lithoshpere, *Tectonophysics*, *136*, 27–63, 1987.

Christensen, N. I., Poisson's ration and crustal seismology, *J. Geophys. Res.*, *101*, 3139–3156, 1996.

Christensen, N. I., and W. D. Mooney, Seismic velocity structure and composition of the continental crust: A global view, *J. Geophys. Res.*, *100*, 3047–3054, 1995.

Das, S., and C. Scholtz, Off-fault aftershock clusters caused by shear stress increase?, *Bull. Seismol. Soc. Am.*, *71*, 1669–1675, 1981.

De Mets, C., R. G. Gordon, D. F. Argus, and S. Stein, Effect of recent revisions to the geomagnetic reversal time scale on estimates of current plate motions, *Geophys. Res. Lett.*, *21*, 2191–2194, 1994.

Dieterich, J. H., A constitutive law for the rate of earthquake production and its application to earthquake clustering, *J. Geophys. Res.*, *99*, 2601–2618, 1994.

Dieterich, J. H., and B. Kilgore, Implications of fault constitutive properties for earthquake prediction, *Proc. Natl. Acad. Sci. U. S. A.*, *93*, 3787–3794, 1996.

Ellsworth, W. L., Earthquake history, 1769–1989, in *The San Andreas Fault System, California*, edited by R. E. Wallace, *U.S. Geol. Surv. Prof. Pap.*, *1515*, 153–187, 1990.

Furlong, K. P., and D. Verdonck, Three-dimensional lithospheric kinematics in the Loma Prieta region, California: Implications for the earthquake cycle, *U.S. Geol. Surv. Prof. Pap.*, *1550-F*, 103–131, 1994.

Geist, E. L., and D. J. Andrews, Slip rates on San Francisco Bay area faults from anelastic deformation of the continental lithosphere, *J. Geophys. Res.*, *105*, 25,543–25,552, 2000.

Hansen, F. D., and N. L. Carter, Semibrittle creep of dry and wet Westerly granite at 1000 MPa, *Proc. U.S. Symp. Rock Mech.*, 24*th*, 429–447, 1983.

Harris, R. A., Introduction to special section: Stress triggers, stress shadows, and implications for seismic hazard, *J. Geophys. Res.*, *103*, 24,347–24,358, 1998.

Harris, R. A., and R. W. Simpson, Suppression of large earthquakes by stress shadows: A comparison of Coulomb and rate-and-state failure, *J. Geophys. Res.*, *103*, 24,439–24,452, 1998.

Henstock, T. J., A. Levander, and J. A. Hole, Deformation in the lower crust of the San Andreas fault system in northern California, *Science*, *278*, 650–653, 1997.

Hill, D. P., J. P., Eaton, and L. M., Jones, Seismicity, 1980–86, in *The San Andreas Fault System, California*, edited by R. E. Wallace, *U.S. Geol. Surv. Open Prof. Pap. 1515*, 115–152, 1990.

Holbrook, W. S., T. M. Brocher, U. S. ten Brink, and J. A. Hole, Crustal structure beneath the San Francisco Bay block and the central California margin, *J. Geophys. Res.*, *101*, 22,311–22,334, 1996.

Hole, J. A., T. M. Brocher, S. L. Klemperer, T. Parsons, H. M. Benz, and K. P. Furlong, Three-dimensional seismic velocity structure of the San Francisco Bay area, *J. Geophys. Res*, *105*, 13,859–13,874, 2000.

Kenner, S., and P. Segall, Time-dependence of the stress shadowing effect and its relation to the structure of the lower crust, *Geology*, *27*, 119–122, 1999.

Kirby, S. H., and A. K. Kronenberg, Rheology of the lithosphere: Selected topics, *Rev. Geophys.*, *25*, 1219–1244, 1987.

Lachenbruch, A. H., and P. Morgan, Continental extension, magmatism, and elevation: Formal relations and rules of thumb, *Tectonophysics*, *174*, 39–62, 1990.

Lachenbruch, A. H., and J. H. Sass, Heat flow and energetics of the San Andreas fault zone, *J. Geophys. Res.*, *85*, 6185–6222, 1980.

Lisowski, M., J. C. Savage, and W. H. Prescott, The velocity field along the San Andreas fault in central and southern California, *J. Geophys. Res.*, *96*, 8369–8389, 1991.

Miller, S. A., Fluid-mediated influence of adjacent thrusting on the seismic cycle at Parkfield, *Nature*, *382*, 799–802, 1996.

Nur, A., and G. Mavko, Postseismic viscoelastic rebound, *Science*, *183*, 204–206, 1974.

Okada, Y., Internal deformation due to shear and tensile faults in a half-space, *Bull. Seismol. Soc. Am.*, *82*, 1018–1040, 1992.

Page, B. M., Tectonic setting of the San Francisco Bay Region, in *Proceedings on the Second Conference on Earthquake Hazards in the eastern San Francisco Bay Area*, edited by G. Borchardt, *Spec. Publ. Calif. Div. Mines Geol.*, *113*, 1–7, 1992.

Parsons, T., and P. E. Hart, Dipping San Andreas and Hayward faults revealed beneath San Francisco Bay, California, *Geology*, *27*, 839–842, 1999.

Parsons, T., R. S. Stein, R. W. Simpson, and P. A. Reasenberg, Stress sensitivity of fault seismicity: A comparison between limited-offset oblique and major strike-slip faults, *J. Geophys. Res.*, *104*, 20,183–20,202, 1999.

Pollitz, F. F., Viscoelastic shear zone model of a strike-slip earthquake cycle, *J. Geophys. Res.*, *106*, 26,541–26,560, 2001.

Prescott, W. H., J. C. Savage, J. L. Svarc, and D. Manaker, Deformation across the Pacific–North America plate boundary near San Francisco, California, *J. Geophys. Res.*, *106*, 6673–6682, 2001.

Reasenberg, P. A., and R. W. Simpson, Response of regional seismicity to the static stress change produced by the Loma Prieta earthquake, *Science*, *255*, 1687–1690, 1992.

Reches, Z., G. Schubert, and C. Anderson, Modeling of periodic great earthquakes on the San Andreas fault: Effects of nonlinear crustal rheology, *J. Geophys. Res.*, *99*, 21,983–22,000, 1994.

Savage, J. C., and M. Lisowski, Inferred depth of creep on the Hayward fault, central California, *J. Geophys. Res.*, *98*, 787–793, 1993.

Savage, J. C., and W. H. Prescott, Asthenospheric readjustment and the earthquake cycle, *J. Geophys. Res.*, *83*, 3369–3376, 1978.

Savage, J. C., J. L. Svarc, and W. H. Prescott, Geodetic estimates of fault slip rates in the San Francisco Bay area, *J. Geophys. Res.*, *104*, 4995–5002, 1999.

Simpson, R. W., Watching the Hayward fault, *Science*, *289*, 1147–1148, 2000.

Simpson, R. W., and P. A. Reasenberg, Earthquake-induced static-stress changes on central California faults, *U.S. Geol. Surv. Prof. Pap.*, *1550-F*, 55–89, 1994.

Stein, R. S., The role of stress transfer in earthquake occurrence, *Nature*, *402*, 605–609, 1999.
Stein, R. S., and M. Lisowski, The 1979 Homestead Valley earthquake sequence, California: Control of aftershocks and postseismic deformation, *J. Geophys. Res.*, *88*, 6477–6490, 1983.
Stein, R. S., A. A. Barka, and J. H. Dieterich, Progressive failure on the North Anatolian fault since 1939 by earthquake static stress triggering, *Geophys. J. Int.*, *128*, 594–604, 1997.
Thatcher, W., Nonlinear strain buildup and the earthquake cycle on the San Andreas Fault, *J. Geophys. Res.*, *88*, 5893–5902, 1983.
Thatcher, W., G. Marshall, and M. Lisowski, Resolution of fault slip along the 470-km-long rupture of the great 1906 San Francisco earthquake and its implications, *J. Geophys. Res.*, *102*, 5353–5367, 1997.
Wang, C., and Y. Cai, Sensitivity of earthquake cycles on the San Andreas fault to small changes in regional compression, *Nature*, *388*, 158–161, 1997.
Wang, C., Y. Cai, and D. L. Jones, Predicting the areas of crustal faulting in the San Francisco Bay region, *Geology*, *23*, 771–774, 1995.
Williams, S. D. P., Current motion on faults of the San Andreas system in central California inferred from recent GPS and terrestrial survey measurements, Ph.D. thesis, Univ. of Durham, Durham, England, 1995.
Working Group on California Earthquake Probabilities, Probabilities of large earthquakes in the San Francisco Bay region, California, *U. S. Geol. Surv. Circ.*, *1053*, 51 pp., 1990.
Working Group on California Earthquake Probabilities, Earthquake probabilities in the San Francisco Bay region: 2000 to 2030—A summary of findings, *U.S. Geol. Surv. Open File Rep.*, *99-517*, 1999.
Yamashina, K., Induced earthquakes in the Izu Peninsula by the Izu-Hanto-Oki earthquake of 1974, Japan, *Tectonophysics*, *51*, 139–154, 1978.
Zoback, M. D., State of stress and crustal deformation along weak transform faults, *Philos. Trans. R. Soc. London, Ser. A*, *337*, 141–150, 1991.

T. Parsons, U.S. Geological Survey, MS-999, 345 Middlefield Road, Menlo Park, CA 94025, USA. (tparsons@usgs.gov)